

Spectral Approaches for the Fast Computation of Yield Surfaces and First-Order Plastic Property Closures for Polycrystalline Materials with Cubic-Triclinic Textures

Hamad F. Al-Harbi¹, Marko Knezevic^{1,2}, and Surya R. Kalidindi^{1,3}

Abstract: In recent work, we have demonstrated the viability and computational advantages of DFT-based spectral databases for facilitating crystal plasticity solutions in face-centered cubic (fcc) metals subjected to arbitrary deformation paths. In this paper, we extend and validate the application of these novel ideas to body-centered cubic (bcc) metals that exhibit a much larger number of potential slip systems. It was observed that the databases for the bcc metals with a larger number of slip systems were more compact compared to those obtained previously for fcc metals with a smaller number of slip systems. Furthermore, we demonstrate in this paper that these databases can be effectively used in the fast computation of yield surfaces predicted by the Taylor model for both fcc and bcc metals. As another demonstration of the many advantages of the novel DFT-based spectral databases, we present first-order plastic property closures based on the Taylor model for both fcc and bcc metals. This paper represents the first report of such closures produced without invoking any simplifying assumptions regarding sample symmetry.

Keywords: crystal plasticity models, spectral method, yield surfaces, First-order closures

1 Introduction

Property closures delineate the complete set of all theoretically achievable combinations of selected effective (anisotropic) properties in a given material system and for a selected homogenization theory, and are of great interest in optimizing the performance of engineering components. In general, these are very difficult to compute as they aim to map the complete space of theoretically feasible microstruc-

¹ Department of Materials Science and Engineering, Drexel University, PA 19104

² Scientific Forming Technologies Corporation, 2545 Farmers Drive, Columbus, OH 43235

³ Corresponding author. Department of Mechanical Engineering and Mechanics, Drexel University, PA 19104

tures in the given material system into the property space of interest. Rigorous solutions known as G-closures (Murat and Tartar 1985; Cherkaev 2000; Lurie 2004) exist only for a limited number of problems, mostly restricted to relatively simple defect-insensitive properties and two-dimensional microstructures comprised of isotropic local states. Clearly, the availability of theoretically predicted closures for elastic-plastic properties of polycrystalline materials (where the local states are typically anisotropic) is of tremendous value in the design and development of new materials with enhanced properties or performance characteristics.

In recent years, a novel mathematical framework called Microstructure Sensitive Design (MSD) (Adams *et al.* 2001; Adams *et al.* 2004; Kalidindi *et al.* 2004; Lyon and Adams 2004; Kalidindi *et al.* 2006; Proust and Kalidindi 2006; Fullwood *et al.* 2007; Houskamp *et al.* 2007; Knezevic and Kalidindi 2007; Wu *et al.* 2007; Fast *et al.* 2008) was introduced to establish invertible linkages between material microstructure and its effective properties. One of the main successes of MSD has been the ability to compute efficiently the first-order approximations to property closures (hereafter referred to as first-order closures) for combinations of a broad range of anisotropic elastic-plastic properties exhibited by polycrystalline material systems (Proust and Kalidindi 2006; Knezevic and Kalidindi 2007; Wu *et al.* 2007; Knezevic *et al.* 2008). The first-order closures are approximations to the rigorous G-closures because they utilize only the first-order statistics of the material microstructure. For polycrystalline microstructures, the first-order microstructure statistics reflect the probability density associated with finding a region of a selected crystal lattice orientation at a point thrown randomly into the polycrystalline microstructure (also called 1-point statistics). These first-order statistics for polycrystalline microstructures are generally described through an orientation distribution function (ODF), also commonly referred to as texture (Bunge 1993).

In the MSD framework, the complete space of all theoretically feasible microstructure distribution functions is identified as a microstructure hull (Adams *et al.* 2001; Proust and Kalidindi 2006; Wu *et al.* 2007). For the first-order statistics in polycrystalline microstructures, this essentially constitutes a texture hull that is conveniently expressed using Fourier representations (Adams *et al.* 2001; Proust and Kalidindi 2006; Wu *et al.* 2007; Kalidindi *et al.* 2009). First-order property closures in polycrystalline materials are essentially obtained by mapping the texture hulls into the selected property spaces. In prior work, this has been accomplished using a number of different optimization techniques, including the gradient methods (Proust and Kalidindi 2006), Pareto-front methods (Fullwood *et al.* 2007), and genetic-like algorithms (Knezevic *et al.* 2008).

To the best of our knowledge, all of the previously reported plastic property closures for polycrystalline materials have been established assuming orthorhombic sample

symmetry in the microstructure statistics (i.e. texture). This was largely because of the computational difficulties involved in establishing the effective properties of the polycrystals without the assumption of orthorhombic sample symmetry. As an example, consider the computation of the uniaxial yield strength of the polycrystal. Since most crystal plasticity models (Kalidindi *et al.* 1992) take the imposed deformation as the input and predict the corresponding stress states, it becomes necessary to guess the deformation mode that would result in an uniaxial stress state. Without the assumption of orthorhombic sample symmetry, this search has to take place on at least a four-dimensional surface (equivalent to establishing the yield surface in five-dimensional stress space). However, with the assumption of orthorhombic sample symmetry, the search can be restricted to a single parameter space.

Much of the prior work in this area has been accomplished using generalized spherical harmonics (GSH) (Bunge 1993) as the Fourier basis in representing the structure-property linkages (Adams *et al.* 2001; Proust and Kalidindi 2006). In recent work (Kalidindi *et al.* 2009; Knezevic *et al.* 2009), we have expounded the computational advantages of using discrete Fourier transform (DFT) representations over the GSH representations. The use of fast Fourier transform (FFT) algorithms (Cooley and Tukey 1965; Brigham 1988; Duhamel and Vetterli 1990; Briggs and Henson 1995; Press *et al.* 2002) has produced major computational advantages in the establishment of structure-property linkages in polycrystalline materials using DFT representations instead of GSH representations (Kalidindi *et al.* 2009; Knezevic *et al.* 2009). All of our recent work with these new methods was applied on fcc metals with 12 slip systems. In this paper, we extend the use of DFT representations of structure-property linkages in polycrystalline materials in three important directions: (i) establishment and validation of the spectral crystal plasticity database for deformation of bcc metals with 48 slip systems (which is much higher than the 12 slip systems operating in fcc metals), (ii) fast computation of the yield surfaces for both bcc and fcc metals using crystal plasticity theories in the five-dimensional deviatoric stress space, and (iii) delineation of first-order plastic property closures for both fcc and bcc metals using these yield surfaces while avoiding any simplifying assumptions of sample symmetry. It is emphasized here that these advances have been made possible due to the tremendous computational savings realized in computing DFTs using established (and easily accessible) FFT algorithms.

This paper is organized as follows. We briefly summarize in Section 2 our recently developed DFT-based approach for crystal plasticity computations. We then proceed to build and validate a new DFT-based crystal plasticity database for bcc metals in Section 3. We then demonstrate the application of the DFT databases for the

fast computation of yield surfaces using the Taylor model in Section 4. As a final application of the DFT databases, we demonstrate the construction of several example first-order plastic property closures in Section 5. In particular, we compare and contrast the property closures produced here with those produced previously with the assumption of orthorhombic sample symmetry. We present concluding remarks in Section 6.

2 DFT-based Approach to Crystal Plasticity Computations

The rigid-viscoplastic crystal plasticity model (Asaro and Needleman 1985) used in this work can be described by the following set of equations:

$$\mathbf{D} = \sum_{\alpha} \dot{\gamma}^{\alpha} \mathbf{P}^{\alpha}, \quad \mathbf{P}^{\alpha} = 0.5 (\mathbf{m}^{\alpha} \otimes \mathbf{n}^{\alpha} + \mathbf{n}^{\alpha} \otimes \mathbf{m}^{\alpha}), \quad (1)$$

$$\dot{\gamma}^{\alpha} = \dot{\gamma}_o \left| \frac{\tau^{\alpha}}{s^{\alpha}} \right|^{1/m} \text{sgn}(\tau^{\alpha}), \quad \tau^{\alpha} = \boldsymbol{\sigma}' \cdot \mathbf{P}^{\alpha}. \quad (2)$$

In Eqs. (1) and (2), \mathbf{D} is the applied isochoric stretching tensor, \mathbf{m}^{α} and \mathbf{n}^{α} are the unit vectors identifying the slip direction and the slip plane normal, respectively, for slip system α . Since elastic stretching is not allowed in this model, \mathbf{D} is also the plastic stretching tensor in the sample. The deviatoric component of the Cauchy stress tensor in the crystal, denoted by $\boldsymbol{\sigma}'$, can be evaluated by solving Eqs. (1) and (2). τ^{α} , $\dot{\gamma}^{\alpha}$, and s^{α} represent the resolved shear stress, the shearing rate, and the slip resistance, respectively, on slip system α . The reference value of the shearing rate, $\dot{\gamma}_o$, is taken here as 0.001 sec^{-1} . The strain rate sensitivity parameter denoted by m is taken to be 0.01, which is typical for plastic deformation of most cubic metals at room temperature. The lattice spin tensor \mathbf{W}^* (and the related lattice rotation tensor, \mathbf{R}^*) in the crystalline region is given by

$$\mathbf{W}^* = \dot{\mathbf{R}}^* \mathbf{R}^{*T} = \mathbf{W} - \mathbf{W}^p, \quad \mathbf{W}^p = \sum_{\alpha} 0.5 \dot{\gamma}^{\alpha} (\mathbf{m}^{\alpha} \otimes \mathbf{n}^{\alpha} \otimes \mathbf{n}^{\alpha} \otimes \mathbf{m}^{\alpha}), \quad (3)$$

where \mathbf{W} is the applied spin tensor, and \mathbf{W}^p is the plastic spin tensor. To capture slip hardening, the evolution of the slip resistance with accumulated plastic strain is described phenomenologically by a saturation-type law as

$$s^{\alpha} = h_o \left(1 - \frac{s^{\alpha}}{s_s} \right)^a \sum_{\beta} |\dot{\gamma}^{\beta}|, \quad (4)$$

where h_o , s_s and a denote the slip hardening parameters.

The crystal plasticity computations typically demand significant computational resources because of the low value of m (which makes the resulting system of algebraic equations numerically extremely stiff). In the DFT-based approach (Kalidindi *et al.* 2009; Knezevic *et al.* 2009), we establish computationally efficient representations for the essential functions capturing the solutions to the crystal plasticity theory described above. More specifically, our interest here is in establishing functions such as $\sigma'_{ij}(g, \mathbf{L})$, $W_{ij}^*(g, \mathbf{L})$, and $\sum_{\alpha} |\dot{\gamma}^{\alpha}|(g, \mathbf{L})$, where g is the crystal lattice orientation and \mathbf{L} is the applied velocity gradient tensor. In any given time step in the simulation of the deformation process, these functions can then be used to compute all of the needed microscale and macroscale field quantities that would be typically computed by the traditional crystal plasticity approach (by explicitly solving Eqs. (1)-(4)).

It is important to note that the functions sought here are independent of the specific homogenization theory used in bridging the microscale response of the crystalline regions within individual grains to the macroscale polycrystal response. In the simple extended Taylor models (Taylor 1938) used in this work, the applied velocity gradient tensor at the microscale is assumed to be the same as the one applied at the macroscale (on the polycrystal). In the classical Taylor model, only the strain tensor in each grain is assumed to be the same. However, in both versions of this model, the macroscopic stress for the polycrystal is obtained by volume averaging the stresses inside the polycrystal. In using the spectral databases described here with more sophisticated homogenization theories, it will be necessary to first solve for the local (microscale) velocity gradient tensor to be applied and then use that as input to the functions described above.

The domain of the functions of interest in this work is the product space of the orientation space and the deformation mode space. The orientation, g , may be described using any one of the established representations (Randle and Engler 2000), including Euler angles, angle-axis pairs, Rodriguez vectors, quaternions, or orthogonal matrices. A common feature of these different, but equivalent, representations is that all of them require specification of three independent parameters to describe a given crystal orientation. Consequently, the orientation space of interest can always be reduced to a three-dimensional space. In the present work, we have used the Bunge-Euler representation for orientations (Bunge 1993), where the crystal lattice orientation is typically denoted as $g = (\phi_1, \Phi, \phi_2)$ by a ordered set of three rotation angles that transform the crystal reference frame to the sample reference frame. The orientation space associated with this representation is usually defined as $(\phi_1 \in [0, 2\pi), \Phi \in [0, \pi), \phi_2 \in [0, 2\pi))$, which could be further compacted significantly by taking advantage of any prevailing crystal and sample symmetries in a given material system (Bunge 1993).

The deformation mode space of interest here includes the complete set of all velocity gradient tensors that can be imposed on the selected material system. In building the DFT-based spectral databases needed for crystal plasticity solutions, we successfully employed a strategy developed by Van Houtte (Van Houtte 1994) for compacting the deformation mode space. For this purpose, the velocity gradient tensor is mathematically decomposed as

$$\mathbf{L} = \dot{\epsilon} \mathbf{D}_o + \mathbf{W}, \quad \mathbf{D}_o = \sum_{j=1}^3 \mathbf{D}_j e_j^p \otimes e_j^p, \quad \dot{\epsilon} = |\mathbf{D}|, \quad (5)$$

$$D_1 = \sqrt{\frac{2}{3}} \cos\left(\theta - \frac{\pi}{3}\right), \quad D_2 = \sqrt{\frac{2}{3}} \cos\left(\theta + \frac{\pi}{3}\right), \quad D_3 = -\sqrt{\frac{2}{3}} \cos(\theta),$$

where $\{e_i^p, i = 1, 2, 3\}$ denotes the principal frame of \mathbf{D}_o , and the range of angular variable θ that defines all possible diagonal matrices is $[0, 2\pi)$. However, since there are multiple choices for the selection of the principal frame, a restricted range of $[\frac{\pi}{6}, \frac{\pi}{2})$ can generate unique representations for all possible tensors \mathbf{D} . Recognizing that all crystal plasticity computations can be performed in the $\{e^p\}$ reference frame allows us to focus our efforts in building the spectral databases using two primary variables, g^p and θ , where g^p denotes the crystal lattice orientation with respect to the $\{e^p\}$ reference frame. As a consequence of this compaction, the domain for the functions of interest here is the product space of the domains for g^p and θ . In other words, we only need to establish the following spectral representations for our work (Knezevic *et al.* 2009)

$$\mathbf{W}_{rq}^* = \dot{\epsilon} \frac{1}{N_g N_\theta} \sum_k \sum_n \mathbf{B}_{kn} e^{\frac{2\pi i k r}{N_g}} e^{\frac{2\pi i n q}{N_\theta}} + \mathbf{W}, \quad (6)$$

$$\sigma'_{rq} = s |\dot{\epsilon}|^m \text{sgn}(\dot{\epsilon}) \frac{1}{N_g N_\theta} \sum_k \sum_n \mathbf{C}_{kn} e^{\frac{2\pi i k r}{N_g}} e^{\frac{2\pi i n q}{N_\theta}}, \quad (7)$$

$$\left(\sum_\alpha |\dot{\gamma}^\alpha| \right)_{rq} = |\dot{\epsilon}| \frac{1}{N_g N_\theta} \sum_k \sum_n G_{kn} e^{\frac{2\pi i k r}{N_g}} e^{\frac{2\pi i n q}{N_\theta}}. \quad (8)$$

In Eqs. (6)-(8), r and q enumerate the grid points in the orientation space (domain of g^p) and the θ space (describing the deformation mode), respectively, while N_g and N_θ represent the corresponding total number of grid points in the same spaces. The sets of Fourier coefficients \mathbf{B}_{kn} , \mathbf{C}_{kn} , and G_{kn} are generally referred to as the DFTs, and constitute the spectral databases needed for facilitating the fast crystal plasticity solutions described here.

In order to compute the DFTs of interest, we first need to compute the values of the functions of interest on a uniform grid in their respective periodic domains. In

this work, these values were computed using the crystal plasticity theory described earlier on a uniform three-degree grid in each of the angular variables involved. The periodic Bunge-Euler space of interest in computing DFTs for orientation-dependent functions in cubic crystals is identified as

$$(\phi_1 \in [0, 2\pi), \Phi \in [0, 2\pi), \phi_2 \in [0, 2\pi))$$

(Kalidindi *et al.* 2009; Knezevic *et al.* 2009). The periodic space of interest in defining the deformation mode is identified as $\theta \in [0, 2\pi)$. It should be noted that there exist several redundancies in the space identified above; in fact, there exist at least 48 equivalent orientations based on the crystal symmetry alone. These equivalent representations have been exploited in the computations of the function values.

For the functions studied in this work, it is typically observed that only a small fraction of the DFTs are numerically significant compared to the others. In other words, although the number of DFTs computed is as large as the discrete dataset of the function values that was used in computing the transform, only a relatively small fraction of the terms in the computed transform need to be stored; ignoring the rest of the terms in the transform has only a small influence on the reconstructed values. The numbers of numerically significant DFTs (henceforth referred to as dominant DFTs) varies for the different field variables. It was seen that as few as 200 DFTs dominated the representations of the various functions of interest for fcc polycrystals (Knezevic *et al.* 2009). Keeping a minimal set of dominant DFTs is critical for gaining computational speed in the spectral approach to the crystal plasticity computations described in this paper. Taking into account more of the DFTs will improve the accuracy at the expense of computational cost.

A characteristic feature of the DFTs is that they reproduce exactly the values of the functions at the grid points that were used in evaluating the DFTs (here the uniform three degree grid), when all of the DFTs are utilized. In order to recover the function values at any other location of interest (not on the selected grid) in their respective domains, we use the spectral interpolation technique described in our earlier work (Knezevic *et al.* 2008).

3 Spectral Databases for BCC metals

Following the approach described in the previous section, we have developed in this work a new spectral database for deformation of bcc metals with 48 slip systems. The families of potential slip systems for the bcc crystals are assumed to include $\{110\}\langle\bar{1}11\rangle$, $\{\bar{1}12\}\langle1\bar{1}1\rangle$, and $\{12\bar{3}\}\langle111\rangle$. The DFTs of interest representing the functions described in Eqs. (6)-(8) were computed using the same procedures

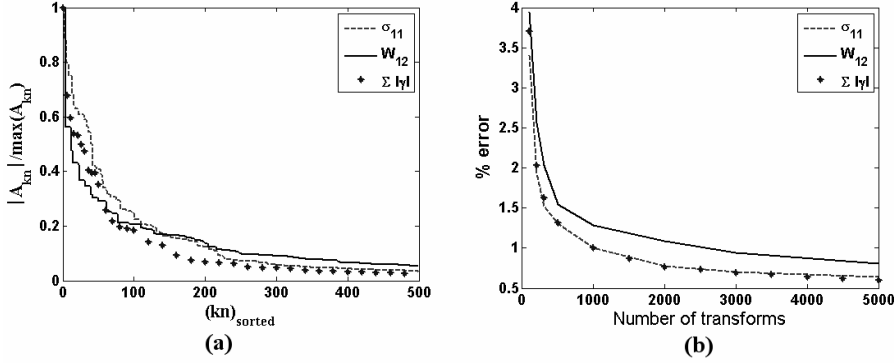


Figure 1: (a) Magnitudes of dominant transforms (not including the zero transform) normalized by the largest value and sorted by magnitude for the components $\sigma'_{11}(g^p, \theta)$, $W_{12}^*(g^p, \theta)$, and $\sum_{\alpha} |\gamma^\alpha|(g^p, \theta)$, where A_{kn} here indicates the dominant DFTs. (b) Average percentage error for the same three components computed using Eq. (9) for different numbers of dominant DFTs retained in the computations for 100,000 combinations of selected orientations and deformation modes.

that were used earlier for fcc metals. Fig. 1(a) shows the magnitude of the DFTs (not including the zero transform) for $\sigma'_{11}(g^p, \theta)$, $W_{12}^*(g^p, \theta)$, and $\sum_{\alpha} |\gamma^\alpha|(g^p, \theta)$ normalized by the largest transform for each component and sorted by the magnitude. It is clear from Fig. 1(a) that it should be possible to represent any of the three functions shown with only a few dominant DFTs with only a tolerable loss of accuracy. The accuracy of the spectral representation of the functions using only a limited number of dominant transforms was evaluated using an error metric defined as

$$e = \frac{1}{N} \sum_{i=1}^N \frac{|f_i - f_i^{DFT}|}{f^n} \times 100 \quad (9)$$

where f_i and f_i^{DFT} denote the values of the function of interest computed at N selected locations in the domain of the function using the classical crystal plasticity approach and the spectral approach described here (using Eqs. (6)-(8) and only the dominant DFTs), respectively, and f^n is an appropriate normalization value. In the present work, the normalization value has been taken to be three times the initial slip resistance ($3s_0$) for the deviatoric stress components, and $3\dot{\epsilon}$ for the spin tensor components and the total shearing rate. The locations where the functions were evaluated included a total of 100,000 distinct combinations of g^p and θ , distributed randomly in their respective fundamental zones. The errors computed from Eq.

(9) for $\sigma'_{11}(g^p, \theta)$, $W_{12}^*(g^p, \theta)$, and $\sum_{\alpha} |\dot{\gamma}^{\alpha}|(g^p, \theta)$ are plotted against the number of dominant DFTs retained in the computation of f_i^{DFT} in Fig. 1 (b). The average error when using 500 dominant DFTs was less than 2% for all of these three components. Similar results were also obtained for all the five independent components of the deviatoric stress function and the three independent components of the spin function studied here. It was also observed that the errors noted here for the DFT-based spectral databases for bcc metals were lower than the corresponding errors reported in our earlier work on fcc metals (Knezevic *et al.* 2009). For example, when using 500 dominant DFTs for the deviatoric stress component $\sigma'_{11}(g^p, \theta)$ with the fcc database, the corresponding error was about 2.5%, while it is around 1.5% for the bcc database developed here. We attribute the more compact representation of the functions for bcc crystals obtained here to the availability of many more potential slip systems, compared to the fcc crystals. The availability of the larger number of slip systems results in the functions of interest becoming more uniform in their respective domains, and therefore needs lesser numbers of dominant DFTs to achieve the desired accuracy.

The new bcc spectral database developed here was validated by comparing the predictions of the stress-strain curves and the deformed textures against the corresponding predictions from the conventional crystal plasticity computations for different deformation processes with different initial textures. Both of these predictions are based on the simple Taylor model described earlier. The slip hardening parameters used in these simulations were those established previously for interstitial-free (IF) steel by curve fitting the Taylor predictions to experimental measurements (Peeters *et al.* 2001). The values of these slip hardening parameters were $h_o = 500$ MPa, $s_s = 230$ MPa, $a = 2.80$, and $s_o = 50$ MPa. As an example, the predicted texture and stress-strain curves for a polycrystalline IF steel deformed by simple shear to a shear strain of $\gamma = 0.6$ using the conventional computational approach and the new DFT spectral approach presented in this paper are shown in Fig. 2. The initial texture in the sample was captured using a set of 1200 discrete crystal orientations (Peeters *et al.* 2001). The DFT-based predictions used 500 dominant DFTs for the stress, the shearing rate, and the lattice spin components. It is clear that the DFT-based databases developed here for bcc crystals produce excellent predictions, and these are obtained at a significant faster computational speed. The simulation time was 130 secs for the conventional calculations, and only 2.9 secs for the spectral approach using dominant DFTs. All of the computations reported in this work were performed on a regular Pentium 4 desktop PC.

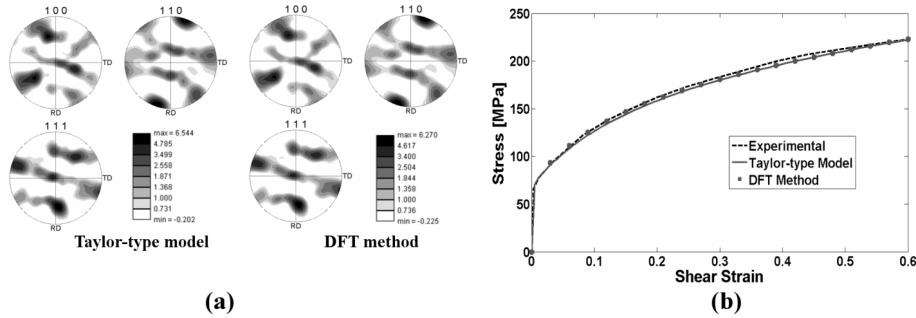


Figure 2: Comparison of the predictions from the spectral method (using 500 DFTs for the stress, the shearing rate, and the lattice spin components) against the corresponding predictions from the conventional approach for simple shear of IF steel: (a) pole figures, and (b) stress-strain curves, including the experimental result (Peeters et al. 2001).

4 Fast Computation of Yield Surfaces using Spectral Databases

The delineation of the anisotropic yield surface in stress space using the Taylor polycrystal model is computationally very expensive. We describe here a new method for the fast computation of the yield surface in the five-dimensional deviatoric stress space using the DFT-based databases developed here as well as in previous work (Knezevic *et al.* 2009).

The distribution of the crystal lattice orientations in a polycrystalline sample can be captured by an orientation distribution function (ODF). The ODF, denoted as $f(g)$, reflects the normalized probability density associated with occurrence of the crystallographic orientation, g , in the sample. ODF is formally defined as

$$f(g)dg = \frac{N_{g \pm dg/2}}{N}, \int_{FZ} f(g)dg = 1, \quad (10)$$

where N is the total number of orientations measured in the sample, $N_{g \pm dg/2}$ is the number of orientations that lie within an invariant measure dg centered about the orientation g , and FZ denotes the fundamental zone of distinct orientations in a suitable defined orientation space. The orientation, g , is defined here using the three Bunge-Euler angles $g = (\phi_1, \Phi, \phi_2)$ (Bunge 1993). The invariant measure is then defined as

$$dg = \sin \Phi d\phi_1 d\Phi d\phi_2 \quad (11)$$

In this work, it is convenient to establish the DFT representation for texture as (Kalidindi *et al.* 2009)

$$\tilde{F}_k = \sum_b f_b \sin \Phi_b e^{\frac{-2\pi i k b}{N_g}} \quad (12)$$

where f_b represents the value of the ODF at the grid point in the orientation space enumerated by b , and \tilde{F}_k denote the corresponding DFTs.

In the Taylor model (Taylor 1938), the macroscopic deviatoric stress tensor, $\bar{\sigma}'$, is given by the volume averaged value of the local stress tensors in the constituent crystals of the polycrystalline aggregate. The volume-averaged value can be efficiently evaluated using Eqs. (7) and (12), and the orthogonal properties of the spectral representations. It can be shown that

$$\bar{\sigma}'_q = s |\dot{\epsilon}|^m \text{sgn}(\dot{\epsilon}) \frac{1}{N_g N_\theta} \sum_k \sum_n \tilde{F}_k \mathbf{C}_{kn} e^{\frac{2\pi i n q}{N_\theta}} \quad (13)$$

where $\bar{\sigma}'_q$ denotes the components of the volume averaged deviatoric stress tensor evaluated on a uniform grid in θ , with the grid points enumerated by q .

Recognizing once again that only a limited number of the \mathbf{C}_{kn} transforms need to be accounted in evaluating Eq. (13) leads to a very efficient computations. Using this relation, the points on the yield surface corresponding to a selected choice of the principle frame of \mathbf{D} are established. However, to establish the complete yield surface in the sample frame, one needs to explore the space of all possible principle frames. The space of all possible principle frames can be identified using a set of Euler angles, analogous to the Bunge-Euler angles used in the definition of the crystal lattice orientation.

It should be noted that the spectral representations of the ODF and the stress functions in this paper do not implicitly assume any sample symmetry. Consequently, the yield surface can be constructed for any texture in the sample, without the need to invoke any simplifying assumptions of sample symmetry. This approach has been used here successfully to construct the complete five-dimensional yield surface for both fcc and bcc polycrystalline materials. Fig. 3(a) represents a selected projection of the five-dimensional yield surface computed here for IF-steel using 500 dominant DFTs. The material was assumed to possess a random texture described by a set of 1000 discrete crystal orientations. The time required for computing the entire five-dimensional yield surface (involving computations of the values of 7,200,000 stress tensors) was only 170 seconds. In order to check the accuracy of the yield surface, we compare in Fig. 3(b) the $(\sigma_{11}, \sigma_{22})$ section of the IF-steel yield surface computed using 500 dominant DFTs against the one computed us-

ing the conventional approach. It is clear that the DFT-based computations are in excellent agreement with the conventional computations.

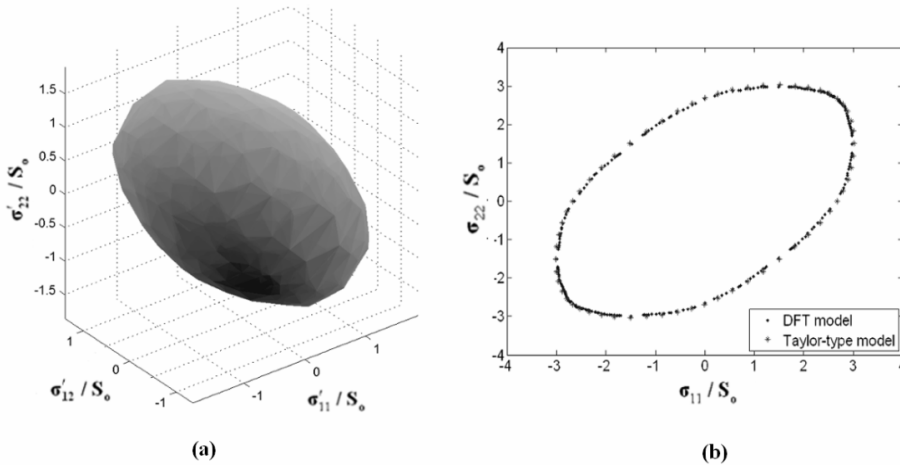


Figure 3: (a) Three-dimensional projection of the yield surface computed using the DFT-based spectral method for IF-steel with a random texture; (b) Plots of the predicted $(\sigma_{11}, \sigma_{22})$ -yield locus for the same material comparing the spectral approach with the conventional Taylor approach.

In order to demonstrate the applicability of the spectral methods described here to fcc metals, we show in Fig. 4 the yield loci in the π -plane for polycrystalline copper computed using 500 dominant DFTs from the fcc database and the corresponding predictions from the conventional calculations. In this example, the metal was assumed to possess a texture that is typically observed in rolled fcc samples. In this work this texture was described by a set of 1000 discrete orientations, which was obtained by simulating plane strain compression to a true strain of -1.0 on an initially random texture. It was seen once again that the DFT method can reproduce all of the features of the conventional computations for this strongly textured sample.

5 Plastic closures for cubic-triclinic textures

The MSD approach to the delineation of first-order property closures using various optimization techniques has been discussed in prior work (Proust and Kalidindi 2006; Knezevic and Kalidindi 2007; Wu *et al.* 2007; Knezevic *et al.* 2008). Note that all of the plastic properties addressed in prior work were associated with cubic-orthorhombic textures (in this standard notation the first symmetry refers to crystal

symmetry and the second one refers to the sample symmetry) in the samples. As mentioned earlier, this was mainly because of the computational difficulties involved in evaluating the properties for cubic-triclinic textures.

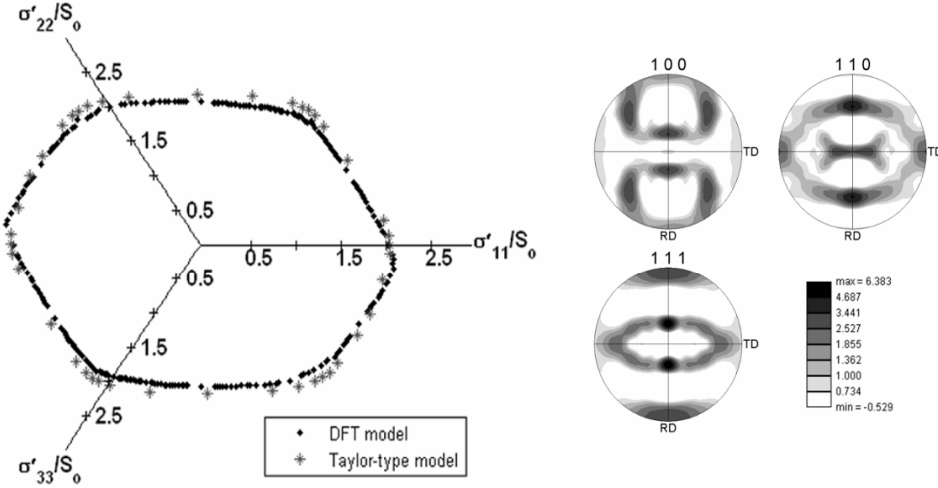


Figure 4: Plots of yield surface on the π -plane computed using the spectral methods described in this work and the conventional approach for polycrystalline fcc copper. The texture in the sample was assumed to be representative of textures found in rolled fcc samples and is shown on the right.

The typical plastic properties of interest such as the tensile yield strength are defined in the stress space. In order to establish these one typically has to guess the imposed deformation mode (i.e. stretching tensor, \mathbf{D}) that would correspond to the stress state of interest. This is most conveniently computed for cubic-triclinic textures by establishing the yield surface. Any other iterative method designed to establish these properties is essentially equivalent to establishing the yield surface in the vicinity of the stress state of interest. In this work, we utilized the methods described in the previous section for the fast computation of the yield surface and produced for the first time a new class of plastic property closures that include cubic-triclinic textures. It should be emphasized that the highly efficient computation of the yield surface using the DFT databases described in the previous section allows us to establish these plastic property closures.

The methodology used here for building the first-order plastic closures follows the genetic-like algorithms described in our prior work (Knezevic *et al.* 2008). The

property combinations of interest were first evaluated for a set of crystal orientations that are uniformly distributed over the entire FZ. In the next step, weighted combinations of crystal orientations located on the boundary were used to expand the property closure. The process was repeated until the closure did not expand any more.

One of our main interests here is to examine critically the differences in the plastic property closures for cubic-orthorhombic and cubic-triclinic textures for both fcc and bcc metals. Although the cubic-orthorhombic closures are expected to be subsets of the cubic-triclinic closures, it is not at all clear how much bigger are the later compared to the former. Since the property closures denote potential design spaces, it is important to ascertain how the cubic-triclinic closures expand the available design space.

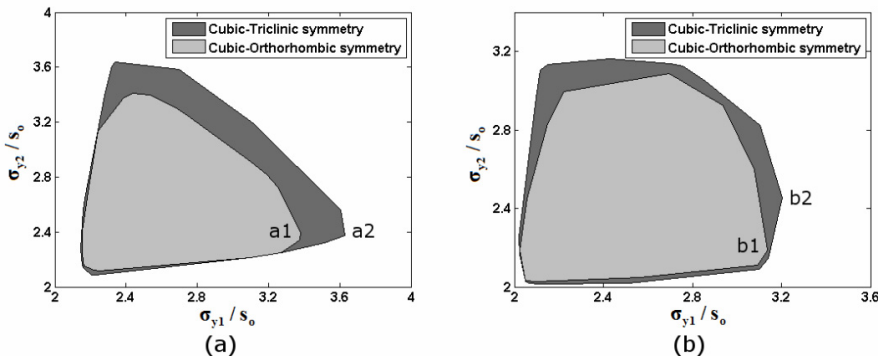


Figure 5: First-order cubic-triclinic and cubic-orthorhombic plastic closures for $(\sigma_{y1}/s_o, \sigma_{y2}/s_o)$ computed using the DFT-based methods developed in this work. (a) OFHC Copper, (b) IF-steel.

In this paper, we computed two example plastic property closures in both fcc copper and bcc IF-steel. Fig. 5 shows the first-order closures delineating all of the feasible combinations of the normalized yield strengths in the sample e_1 and e_2 directions (i.e. σ_{y1} and σ_{y2}) for copper and IF-steel computed assuming both orthorhombic and triclinic sample symmetries. Fig. 5 clearly indicates that some combinations of σ_{y1} and σ_{y2} cannot be attained with the cubic-orthorhombic textures. Comparison of the closures in Figs. 5(a) and 5(b) reveals that the difference between the cubic-orthorhombic and the cubic-triclinic property closures is considerably larger for fcc metals compared to bcc metals. This observation is attributed to the availability of the higher number of slip systems in the bcc metals (48 slip systems in bcc compared to only 12 in the fcc crystals). The higher number of slip systems

are expected to lower the degree of anisotropy in the response of the bcc metals, and should therefore reduce the difference between cubic-orthorhombic and cubic-triclinic closures for these metals compared to the fcc metals.

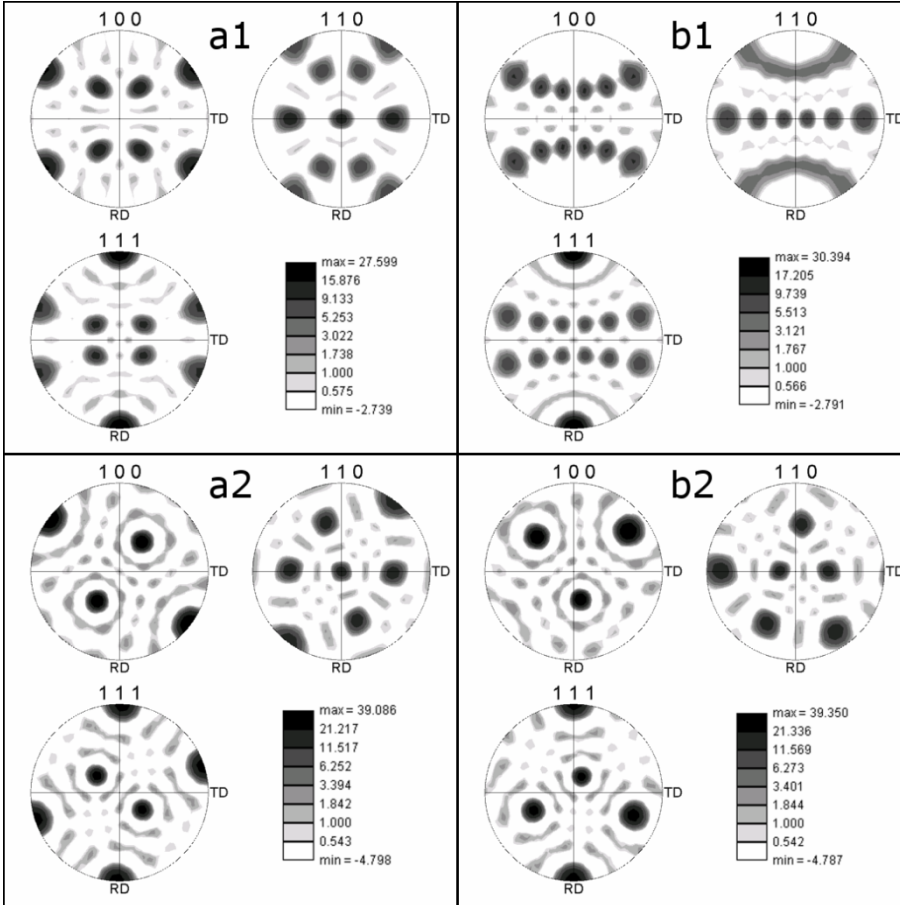


Figure 6: Predicted textures at salient points of interest in Fig. 5 corresponding to the highest values of tensile yield strength, σ_{y1} .

Textures corresponding to the highest values of the tensile yield strengths in Figs. 5(a) and 5(b) are depicted in Fig. 6. It is seen that the highest tensile strength for copper was obtained for a single crystal oriented close to the $(110)[1\bar{1}\bar{1}]$ orientation. However, this single crystal is not represented in the cubic-orthorhombic closure. The highest tensile yield strength in the cubic-orthorhombic closure, based on the Taylor model used here, is obtained by a crystalline aggregate comprising of four

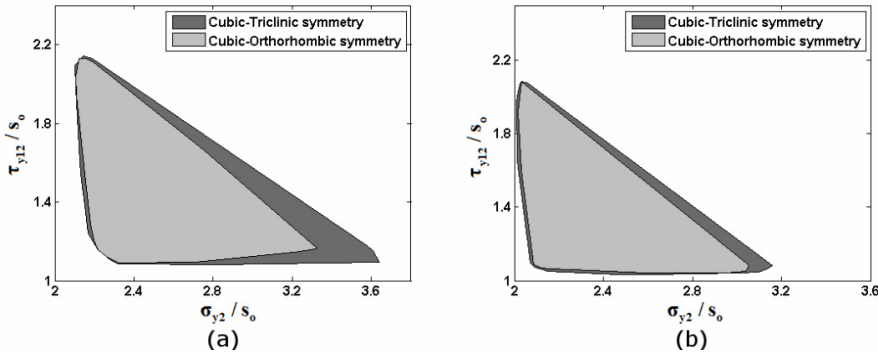


Figure 7: $(\sigma_{y2}/s_0, \tau_{y12}/s_0)$ First-order property closures for polycrystalline materials computed using DFT methods based on cubic-triclinic and cubic-orthorhombic symmetries. a) OFHC Copper, b) IF-steel.

equi-volume crystals that are close to the $(110)\langle 111 \rangle$ orientations. Note that the highest possible tensile yield strength in the orthorhombic closure (for the aggregate comprising four equi-volume crystals) is 7% lower than the corresponding optimum solution in the triclinic closure (for the single crystal). For IF-steel, the orientation corresponding to the highest yield strength was found to be the $(132)[\bar{1}\bar{1}\bar{1}]$ orientation, whereas the highest yield strength with orthorhombic sample symmetry corresponded to a texture that may be visualized as (111) fiber texture with the (111) direction parallel to the tensile loading direction. The difference in their yield strengths was only 3%, somewhat lower than the corresponding difference noted earlier for fcc copper. As noted earlier, the imposition of the orthorhombic sample symmetry had a larger effect on fcc closures compared to the bcc closures. Nevertheless, the results presented here do indicate that relaxing the assumption of orthorhombic sample symmetry increases the design space and identifies new solutions for optimized performance of materials.

As another example, we show first-order cubic-orthorhombic and cubic-triclinic plastic closures for $(\sigma_{y2}, \tau_{y12})$ for both copper and IF steel in Fig. 7. Once again the imposition of the orthorhombic sample symmetry was seen to produce a bigger effect on the fcc closure compared to the bcc closure. The fact that the difference is consistently larger with a lower number of slip systems (i.e. a higher degree of anisotropy) suggests that the effect will be even larger in the case of other lower symmetry crystal structures such as hcp metals.

6 Conclusions

In this study, we have demonstrated significant advances in the formulation and use of computationally efficient DFT representations of structure-property linkages in cubic polycrystalline materials. In particular, we have established the following results:

A new spectral crystal plasticity database using discrete Fourier transforms (DFTs) was established and validated for bcc metals with 48 slip systems. It was seen that a small number of dominant DFTs is enough to capture the dependence of the stresses, the lattice spins, and the total slip rate in individual crystals on their lattice orientation and the applied deformation modes. The DFT-based spectral approach for bcc metals was found to be significantly faster than the conventional crystal plasticity computations.

A new efficient approach was developed for the fast computation of the yield surfaces in the five-dimensional deviatoric stress space for both bcc and fcc metals. This approach was demonstrated in this paper using the Taylor polycrystal plasticity models. This new approach exploited the spectral representations of the texture and the stress function and their orthogonal properties. It was demonstrated that it is possible to construct the entire five-dimensional yield surface at extremely fast computational speeds.

A new class of first-order cubic-triclinic plastic property closures were delineated for the first time for both fcc and bcc metals. This was possible because of the fast computations of the yield surface using the DFT-based approach. It was observed that the assumption of orthorhombic sample symmetry reduces the design space and eliminates some of the optimal solutions in the design of materials with improved performance characteristics. It was also found that the difference in the first-order cubic-orthorhombic and cubic-triclinic plastic closures was higher in fcc metals compared to the bcc metals.

Acknowledgement: The authors gratefully acknowledge financial support received for this work from NSF Grants CMS-0654179 and CMS-0727931.

References

- Adams, B. L., A. Henrie, B. Henrie, M. Lyon, S. R. Kalidindi, H. Garmestani (2001): Microstructure-sensitive design of a compliant beam. *Journal of the Mechanics and Physics of Solids* **49**(8): 1639-1663.
- Adams, B. L., M. Lyon, B. Henrie (2004): Microstructures by design: linear problems in elastic-plastic design. *International Journal of Plasticity* **20**(8-9): 1577-

1602.

Asaro, R. J., A. Needleman (1985): Texture development and strain hardening in rate dependent polycrystals. *Acta Metallurgica et Materialia* **33**(6): 923-953.

Briggs, W. L., V. E. Henson (1995): *The DFT : an owner's manual for the discrete Fourier transform*. Philadelphia, Society for Industrial and Applied Mathematics.

Brigham, E. O. (1988): *The fast Fourier transform and its applications*. Englewood Cliffs, Prentice Hall.

Bunge, H.-J. (1993): *Texture analysis in materials science. Mathematical Methods*. Göttingen, Cuvillier Verlag.

Cherkaev, A. V. (2000): *Variational Methods for Structural Optimization*, Springer, New York.

Cooley, J. W., J. W. Tukey (1965): Algorithm for the machine computation of complex Fourier series. *Mathematics of Computation* **19**: 297-301.

Duhamel, P., M. Vetterli (1990): Fast Fourier Transforms: A Tutorial Review and a State of the Art. *Signal Processing* **19**: 259-299.

Fast, T., M. Knezevic, S. R. Kalidindi (2008): Application of microstructure sensitive design to structural components produced from hexagonal polycrystalline metals. *Computational Materials Science* **43**(2): 374-383.

Fullwood, D. T., B. L. Adams, S. R. Kalidindi (2007): Generalized Pareto front methods applied to second-order material property closures. *Computational Materials Science* **38**(4): 788-799.

Houskamp, J. R., G. Proust, S. R. Kalidindi (2007): Integration of microstructure-sensitive design with finite element methods: Elastic-plastic case studies in FCC polycrystals. *International Journal for Multiscale Computational Engineering* **5**(3-4): 261-272.

Kalidindi, S. R., M. Binci, D. Fullwood, B. L. Adams (2006): Elastic properties closures using second-order homogenization theories: Case studies in composites of two isotropic constituents. *Acta Materialia* **54**(11): 3117-3126.

Kalidindi, S. R., C. A. Bronkhorst, L. Anand (1992): Crystallographic texture evolution in bulk deformation processing of FCC metals. *Journal of the Mechanics and Physics of Solids* **40**(3): 537-569.

Kalidindi, S. R., J. R. Houskamp, M. Lyons, B. L. Adams (2004): Microstructure sensitive design of an orthotropic plate subjected to tensile load. *International Journal of Plasticity* **20**(8-9): 1561-1575.

Kalidindi, S. R., M. Knezevic, S. Niezgod, J. Shaffer (2009): Representation of the orientation distribution function and computation of first-order elastic proper-

- ties closures using discrete Fourier transforms. *Acta Materialia* **57**(13): 3916-3923.
- Knezevic, M., H. F. Al-Harbi, S. R. Kalidindi** (2009): Crystal plasticity simulations using discrete Fourier transforms. *Acta Materialia* **57**(6): 1777-1784.
- Knezevic, M., S. R. Kalidindi** (2007): Fast computation of first-order elastic-plastic closures for polycrystalline cubic-orthorhombic microstructures. *Computational Materials Science* **39**(3): 643-648.
- Knezevic, M., S. R. Kalidindi, D. Fullwood** (2008): Computationally efficient database and spectral interpolation for fully plastic Taylor-type crystal plasticity calculations of face-centered cubic polycrystals. *International Journal of Plasticity* **24**(7): 1264-1276.
- Knezevic, M., S. R. Kalidindi, R. K. Mishra** (2008): Delineation of first-order closures for plastic properties requiring explicit consideration of strain hardening and crystallographic texture evolution. *International Journal of Plasticity* **24**(2): 327-342.
- Lurie, K. A.** (2004): A stable spatio-temporal G-closure and Gm-closure of a set of isotropic dielectrics with respect to one-dimensional wave propagation. *Wave Motion* **40**(2): 95-110.
- Lyon, M., B. L. Adams** (2004): Gradient-based non-linear microstructure design. *Journal of the Mechanics and Physics of Solids* **52**(11): 2569-2586.
- Murat, F., L. Tartar** (1985): Optimality conditions and homogenization. *In: Marino, A., Modica, L., Spagnolo, S., DeGiorgianni, M. (Eds.), Non-linear variational problems, Research Notes in Mathematics, Pitman, London.*
- Peeters, B., M. Seefeldt, C. Teodosiu, S. R. Kalidindi, P. Van Houtte, E. Aernoudt** (2001): Work-hardening/softening behaviour of b.c.c. polycrystals during changing strain paths: I. An integrated model based on substructure and texture evolution, and its prediction of the stress-strain behaviour of an IF steel during two-stage strain paths. *Acta Materialia* **49**(9): 1607-1619.
- Press, W. H., S. A. Teukolsky, W. T. Vetterling, B. P. Flannery** (2002): Numerical Recipes in C++.
- Proust, G., S. R. Kalidindi** (2006): Procedures for construction of anisotropic elastic-plastic property closures for face-centered cubic polycrystals using first-order bounding relations. *Journal of the Mechanics and Physics of Solids* **54**(8): 1744-1762.
- Randle, V., O. Engler** (2000): *Introduction to Texture Analysis. Macrotecture, Microstructure & Orientation Mapping*, Gordon and Breach Science Publishers.
- Taylor, G. I.** (1938): Plastic strain in metals. *Journal of the Institute of Metals* **62**: 307-324.

Van Houtte, P. (1994): Application of plastic potentials to strain rate sensitive and insensitive anisotropic materials. *International Journal of Plasticity* **10**(7): 719-748.

Wu, X., G. Proust, M. Knezevic, S. R. Kalidindi (2007): Elastic-plastic property closures for hexagonal close-packed polycrystalline metals using first-order bounding theories. *Acta Materialia* **55**(8): 2729-2737.